J Mol Model (2005) 11: 69–79
DOI 10.1007/s00894-004-0227-4

ORIGINAL PAPER

Björn Windshügel · Johanna Jyrkkärinne · Antti Poso
Paavo Honkakoski · Wolfgang Sippl

Molecular dynamics simulations of the human CAR ligand-binding domain: deciphering the molecular basis for constitutive activity

Received: 20 August 2004 / Accepted: 2 November 2004 / Published online: 23 December 2004

Abstract The constitutive androstane receptor (CAR) belongs to the superfamily of nuclear-hormone receptors that function as ligand-activated transcription factors. CAR plays an essential role in the metabolism of xenobiotics and shows—in contrast to related receptors—constitutive activity. However, the molecular basis for the constitutive activity remains unclear. In the present study, homology models of the ligand binding domain (LBD) were generated based on the crystal structures of the related pregnane X (PXR) and the vitamin D receptor (VDR). The models were used to investigate the basal activity of CAR and the effect of coactivator binding. Molecular dynamics (MD) simulations of complexed and uncomplexed receptor revealed a hypothesis for the activation mechanism. The suggested mechanism is supported by experimental results from site-directed mutagenesis. The basal activity of CAR can be explained by specific van-der-Waals interactions between amino acids on the LBD and its C-terminal activation domain (AF-2). Docking studies with the GOLD program yielded the interaction modes of structurally diverse agonists, giving insight into mechanisms by which ligands enhance CAR activity.

Keywords Activation mechanism · CAR · Nuclear receptor · GROMACS · Molecular dynamics · GOLD · Docking

Abbreviations CAR: Constitutive androstane receptor · CITCO: (6-(4-chlorophenyl)imidazo[2,1-b][1,3]thiazole-5-carbaldehyde O-(3,4-dichlorobenzyl)oxime · DBD: DNA binding domain · LBD: Ligand binding domain · PXR: Pregnane X receptor · RXR: Retinoid X receptor · SRC-1: Steroid receptor coactivator 1 · TMPP: Tri-*p*-methylphenylphosphate · VDR: Vitamin D receptor

Introduction

The metabolism of xenobiotics such as environmental pollutants, pesticides or drugs involves sequential steps of oxidation, mainly by cytochrome P450s (CYPs) and conjugation by various transferases into hydrophilic, water soluble derivatives that are easily excreted [1–3]. An exposure to xenobiotics also causes an adaptive increase in the expression of metabolic enzymes, termed induction, resulting in a faster inactivation and elimination but sometimes increased toxic reactions or unwanted drug–drug interactions, as shown for CYP3A4 [4, 5]. The constitutive androstane receptor (CAR) [6] and the pregnane X receptor (PXR) [7] are the main regulators of gene expression of metabolizing enzymes in the liver and the intestine. Both CAR and PXR belong to the superfamily of nuclear-hormone receptors. In humans, this superfamily of ligand-activated transcription factors comprises 48 members that are involved in regulation of homeostasis, development, reproduction and metabolism [8]. All receptors share a common topology and are constituted of different functional domains. Typically, a nuclear receptor comprises a N-terminal domain of high variability, a conserved DNA-binding domain (DBD) and a ligand-binding

Dedicated to Prof. Dr. H-D. Höltje on the occasion of his 65th birthday

B. Windshügel (✉) · W. Sippl
Department of Pharmaceutical Chemistry,
Martin-Luther-University,
Halle-Wittenberg, Wolfgang-Langenbeck-Str. 4,
06120 Halle, Saale, Germany
E-mail: windshuegel@pharmazie.uni-halle.de
Tel.: +49-345-5525043
Fax: +49-345-5527355

J. Jyrkkärinne · P. Honkakoski
Department of Pharmaceutics, University of Kuopio,
1627, 70211 Kuopio, Finland

A. Poso
Department of Pharmaceutical Chemistry,
University of Kuopio,
1627, 70211 Kuopio, Finland

domain (LBD) that is attached to the DBD via a linker region. Some receptors show an additional C-terminal region of yet unknown function.

For a number of nuclear receptors, the three-dimensional structure of the LBD has been resolved by X-ray crystallography. The structures revealed a general architecture for nuclear-hormone receptors and how endogenous ligands and xenobiotics interact with the binding site. The common fold of the LBDs comprises a three-layered antiparallel helix sandwich composed of 12 helices and a three-stranded beta-sheet [9]. The ligand-binding pocket is located between the outer layers of the helix sandwich and is mainly formed by hydrophobic amino-acid residues. A prerequisite for the stimulated gene transcription is the formation of receptor dimers that subsequently bind to specific DNA sequences and the binding of a coregulator [10]. For example, PXR and CAR form a heterodimer with the retinoid X receptor (RXR) enabling recognition of several DNA response elements [11]. Coactivator binding to the receptor dimer-DNA-complex prompts the recruitment of other factors. The resulting multicomplex is then responsible for the local decondensation of chromatin. Finally, gene expression is initiated via direct and indirect interaction with the basal transcription machinery [12].

The LBD harbors a short helix (H12, also termed AF-2) within its C-terminus that is responsible for the activation of transcription. Agonists and antagonists are able to modulate the gene activation via induction of a conformational change of AF-2, which in turn dictates complex formation with either coactivators or corepressors. In the case of an agonist-bound receptor, AF-2 covers the ligand-binding pocket like a lid and simultaneously takes part in the formation, together with helix H3 and H4, of a hydrophobic groove. This groove represents the binding site for coactivators [13]. When the receptor binds an antagonist, this groove undergoes a reorientation and excludes AF-2, thus enabling the binding of corepressors.

Unlike classical nuclear receptors, the CAR possesses strong transcriptional activity in the absence of any added ligand [6]. The basal activity of the CAR can be enhanced by agonist binding. However, currently only a few agonists for the human CAR have been described, such as CITCO (6-(4-chlorophenyl)imidazo[2,1-b][1, 3]thiazole-5-carbaldehyde O-(3,4-dichloro-benzyl)oxime) [14] and tri-*p*-methylphenylphosphate (TMPP) [15]. Another CAR ligand, clotrimazole, has given contrasting results [14, 16]. In our own studies clotrimazole acts as a strong activator [17, 18].

In this work, homology models of the human CAR ligand-binding domain alone and in complex with a coactivator were generated since a X-ray crystal structure has not yet been determined. The aim of the modeling study was to elucidate the mechanism of the constitutive activity as well as to analyze the binding mode of known agonists and their effect on the CAR LBD. Our models are based on the crystal structures of the related nuclear receptors PXR and vitamin D receptor (VDR). Despite the common nuclear receptor fold, PXR and VDR also exhibit differences in their architecture, which must be considered during model building [19, 20]. The interactions between CAR, coactivators and ligands were studied using molecular dynamic simulations (MD). Based on these simulations, the essential features responsible for the constitutive activity of CAR were identified and compared with experimental mutagenesis data.

Results

In order to apply the approach of homology modeling, a suitable template structure must be found for the sequence-structure alignment. In the case of the CAR, sequences of the closely related VDR and PXR receptors, of which crystal structures are available, show about 40 and 50% sequence identity within the LBD, respectively. To test the reliability of a homology-modeling procedure using only a single template structure, we generated models of the PXR and VDR LBD and compared them with their X-ray structures. Thus, the VDR homology model is based on the PXR template structure, and vice versa. The sequence identity between PXR and VDR in the LBD is 37%. In contrast to the common topology of nuclear receptors, both the PXR and VDR contain an additional domain inserted between helix H1 and H3. In the case of the PXR, this domain consists of a helical segment and two β-strands. The insertion domain in the X-ray structure of the VDR contains two additional helices and an artificial loop segment. A further deviation from the common topology in PXR occurs in the region of helices H6 and H7. The superimposition of the minimized and equilibrated VDR and PXR models and their corresponding crystal structure revealed large RMSD values, indicating that the strategy based on only one template structure does not yield a reliable receptor model. Therefore, we used a combined approach for the generation of the CAR homology model. P×R was chosen as main template.

In order to account for the structural deviations of PXR, the VDR structure was used as scaffold for modeling the segment between H1 and H3 and helices H6 and H7. Additionally, the proximal helices H10/11 and the AF-2 domain were generated based upon the VDR template. Figure 1a shows the complete sequence alignment as well as the parts taken from each template. In order to analyze the influence of coactivator binding, a second model with the complexed coactivator peptide (named CAR-SRC-1) was built following the procedure described previously. The coordinates for the coactivator were taken from the PXR X-ray structure [21] that had been crystallized with a 15 amino-acid peptide from the steroid-receptor coactivator 1 (SRC-1) carrying the binding motif for nuclear receptors. The MD simulations of both CAR and CAR-SRC-1 models revealed that the overall fold of the nuclear receptors remained stable. The RMSD did not exceed 0.2 nm within the

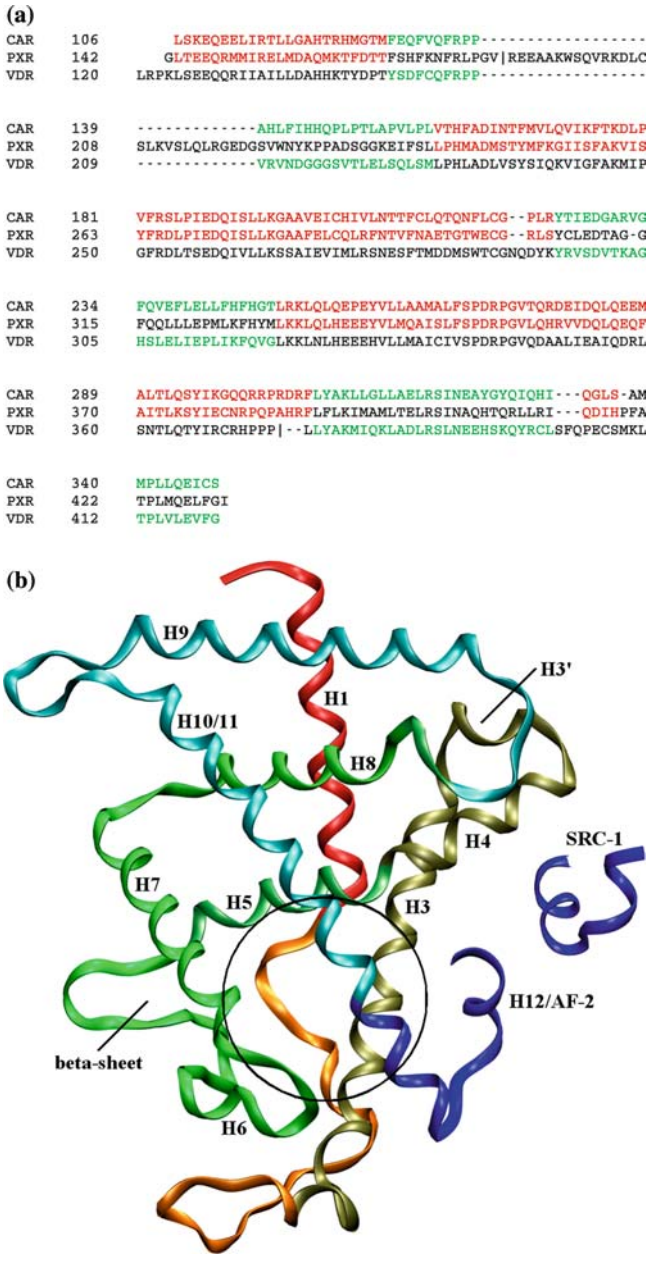

Fig. 1 Homology modeling. **a** Sequence alignment of the two template structures PXR and VDR and the target sequence of CAR. *Vertical lines* indicate missing segments. Residues within the CAR sequence are colored depending on the origin of the structural information used (PXR: *red*, VDR: *green*). **b** Homology model of CAR-SRC-1. Helices are numbered according to the common fold for nuclear receptors. The *circle* indicates the position of the ligand binding pocket

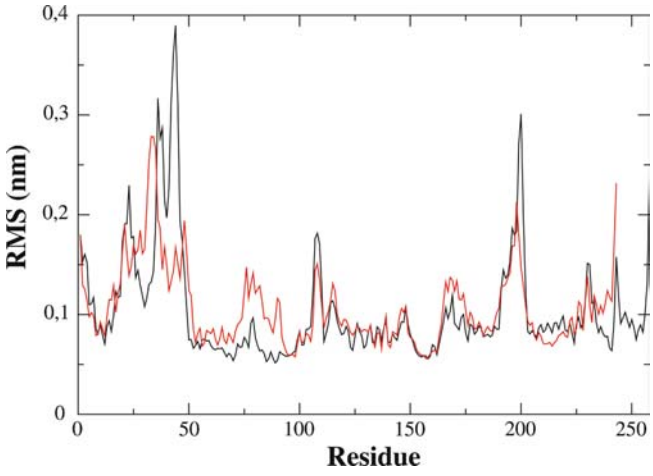

Fig. 2 Analysis of the MD simulation. RMS-fluctuation within the CAR LBD backbone region during MD simulations (color codes: CAR: *red*; CAR-SRC-1: *black*). Loops spanning from H1 to H3 (Residues 11–50) and from H9 to H10/11 (Residues 190–203) show high flexibility in both models

backbone region. This might be due to the compact architecture of the three-layered helix sandwich, which allows only limited motions of the individual domains. The Ramachandran plots for CAR and CAR-SRC-1 models assessed 87.4 and 86.4% of the ψ–ϕ torsion angles as being within the favorable region, respectively. The Profiles-3D-scores for CAR and CAR-SRC-1 models, 98 and 116, are rather or very close to that expected for a high quality model of corresponding size (110 and 117, respectively). To account for the artificial fold taken from VDR and the ensuing additional helix, these segments were not constrained during the MD equilibration. Consistent with secondary structure predictions, this led to an unfolding of the helical segment, resulting in a long disordered loop showing significant changes in RMSD (Fig. 2). In addition, increased flexibility was observed for the loop connecting H9 and H10/11. However, this loop is located at the LBD surface far away from the ligand-binding pocket and the AF-2 domain (Figs. 1b, 3).

The ligand-binding pocket of the CAR is constituted by the helices H3, H5–H7, H10/11 and the beta-sheet connecting helix H5 and H6. The AF-2 domain assumes the active conformation, forming a lid over the binding cavity that is significantly smaller (630 $Å^3$ before and 480 $Å^3$after MD simulation) compared to the binding cavity of the PXR receptor (1294 $Å^3$). As observed for PXR and VDR, the CAR ligand-binding pocket is mainly composed of hydrophobic residues with only a few polar residues contributing.

In both models, the AF-2 domain remained closely attached to the LBD during the entire MD simulation (Fig. 3). It is not expected that a large movement of the AF-2 domain occurs within the time range of the MD simulation performed, however the high stability of the LBD-AF-2 interaction is in close agreement with the experimental data [22, 23]. In the CAR model, strong interactions can be observed between AF-2 and LBD. These could be reproduced in several MD simulations using slightly different starting geometries of the homology model. The aliphatic AF-2 amino acids Leu343 and Ile346 contact with hydrophobic or aromatic residues of the LBD (Val199, Tyr326, Ile330; see Fig. 4a). The importance of these van-der-Waals interactions has also been detected using the GRID program. Using the hydrophobic methyl probe within GRID, we

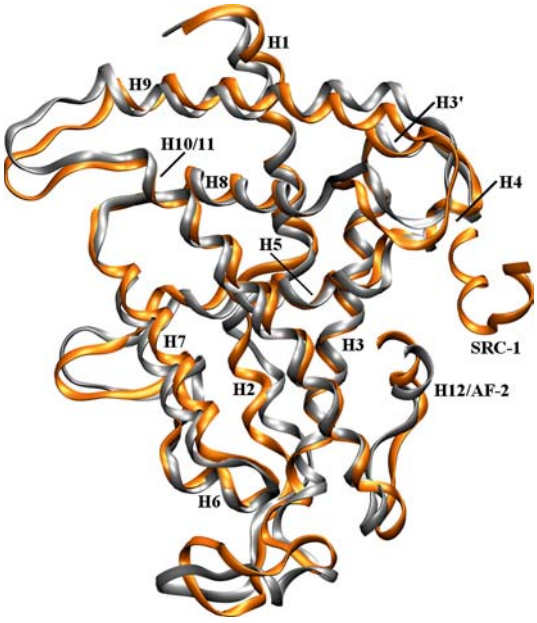

Fig. 3 Comparison of CAR with CAR-SRC-1. Superposition of representative frames from the MD simulations (color code: CAR: *grey*; CAR-SRC-1: *orange*). Structural differences between both models are observed mainly in loop regions. In the model with bound SRC-1 the AF-2 helix is slightly reoriented

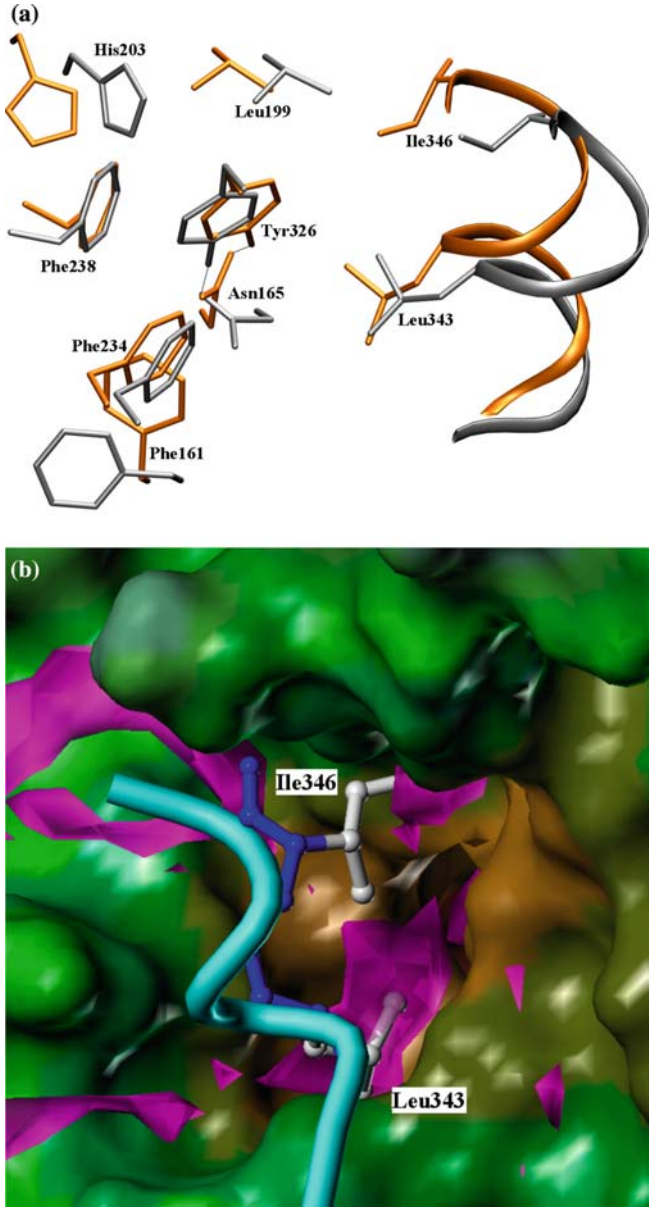

Fig. 4 The constitutive activity. **a** Superposition of CAR (*grey*) and CAR-SRC-1 (*orange*). In both models AF-2 (*tube representation*) interacts via Leu343 with Tyr326 and Ile330 (not shown) located on H10/11 and via Ile346 with Val199 on H4. Various surrounding amino acids stabilize the position of Tyr326 (Val199, His203, Phe234, Phe238 and Ile330). Additionally a hydrogen bond is formed between Asn165 and Tyr326 which has been found to be more stable upon SRC-1 binding. **b** Favorable regions of interactions between the GRID methyl probe and the AF-2 truncated LBD (colored magenta, contour level -2.5 kcal mol^{1}). Only the MOLCAD surface of the LBD is shown, colored according to the lipophilic potential (*blue* polar, *brown* lipophilic). The position of the two hydrophobic residues Leu343 and Ile346 from the AF-2 helix (*colored cyan*) is in close agreement with the obtained GRID results

inspected the interaction possibilities between the LBD and the AF-2 domain. For this purpose, we generated an AF-2-truncated CAR model and calculated the GRID interaction fields. The calculated contour maps were then viewed superimposed on the structure of the complete CAR (Fig. 4b). Two main interaction regions were detected at the LBD-AF-2 interface region by GRID. The location and size of the calculated contour maps is in close agreement with the positions of Leu343 and Ile346 from the AF-2 domain.

Tyr326 is surrounded by a cluster of aromatic or hydrophobic residues (Val199, His203, Phe234, Phe238, Ile330) that seem to fix the position of Tyr326 side-chain. During the MD simulation, a transient hydrogen bond between Tyr326 and Asn165 is formed. Phe161 points into the ligand-binding pocket and interacts with Tyr224. Each of the interactions described between AF-2 and the LBD is also observed in the CAR-SRC-1 model. However, the AF-2 domain is positioned closer to the LBD, (Figs. 3, 4a) allowing contacts between Ile346 and Tyr326 on H10/11. Tyr326 moved towards Leu343, resulting in stronger van-der-Waals interactions (Table 1). The hydrogen bond between Tyr326 and Asn165 appeared to be more stable, as indicated by distance plots (data not shown), resulting in a permanent interaction between H3 and H10/11 in the presence of SRC-1 peptide. Phe161 was reoriented towards the interface between LBD and AF-2, where it forms contacts to LBD residues (Asn165, Phe234, Tyr326) as well as AF-2 (Leu343) and the preceding loop (Met339).

Activation of nuclear receptors requires the binding of coactivators such as SRC-1. The known crystallographic and experimental data reveal that nuclear receptors possess specific interaction patterns for the binding of coactivators [24, 25], which seem to be essential for their function. Thus reproducing the inter-

Table 1 Observed distances (Å) between Tyr326 from the LBD and Leu343/Ile346 from the AF-2 domain in the individual models (see text for further explanation)

	CAR	CAR-SRC-1	CAR-SRC-1 Clotrimazole	CAR-SRC-1 TMPP	Mutation Phe238Ala	Mutation Phe243Ala
Tyr326–Leu343	5.2	4.7	3.9	4.1	9.1	7.9
Tyr326–Ile346	7.3	4.5	4.8	4.6	8.6	8.9

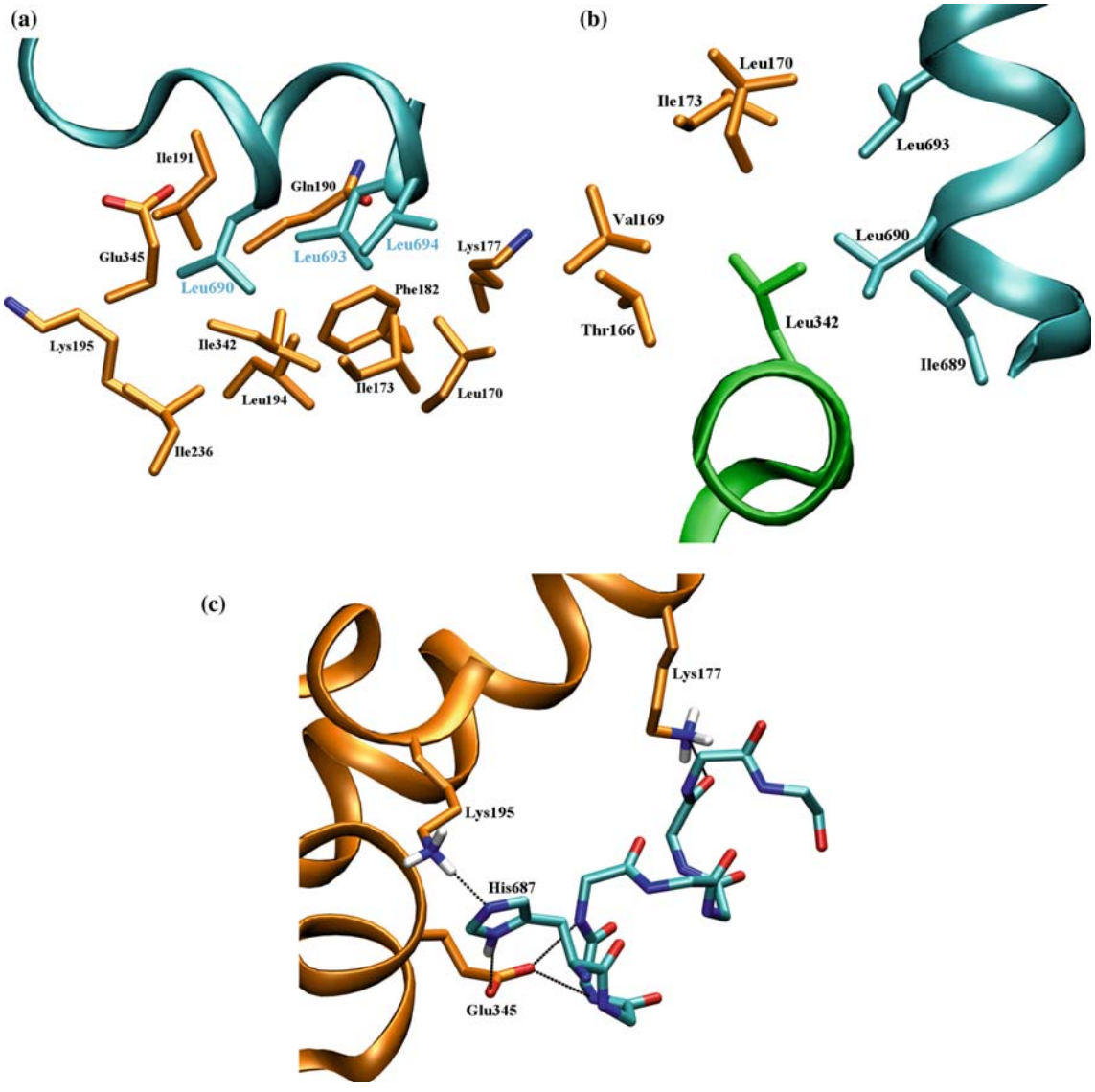

Fig. 5 Interactions between LBD and SRC-1. **a** Several residues from H3, H3′, H4 and AF-2 (carbon atoms in *orange*) form a hydrophobic groove to which SRC-1 (*cyan*) can bind. Leucines from the LxxLL motif on SRC-1 are shown explicitly. **b** Binding of SRC-1 to the LBD fixes Leu342 from AF-2 (*green*) in a hydrophobic pocket formed by several amino acids from LBD (*orange*) and SRC-1 (*cyan*). **c** The helix dipole of SRC-1 is stabilized by Lys177 (H3) and Glu345 (AF-2) located on the LBD (*orange*) forming the so-called "charge clamp". Lys177 interacts via a hydrogen bond with the backbone carbonyl group of Leu693, whereas Glu345 interacts with the backbone nitrogen atoms of Ile689 and Leu690. Also hydrogen bonds are formed between His687 (SRC-1) and Lys195 (H4) as well as His687 and Glu345. Parts of the LBD have been removed to show the interactions more clearly

actions between LBD and coactivator seems to be a prerequisite for a reliable homology model. In crystal structures, the interaction domain of the coactivator adopts an α-helical form and contains the LxxLL motif, which interacts with hydrophobic residues located within a groove formed by the helices H3, H4 and AF-2. In the CAR-SRC-1 model, the hydrophobic groove is formed by 11 residues (shown in Fig. 5a). Leu342 (AF-2) is fixed in a hydrophobic pocket formed by LBD and SRC-1 (Fig. 5b). The helix dipole of the SRC-1 peptide is known to be stabilized by two conserved amino acids interacting with its N-terminal and C-terminal residues that form the so-called "charge-clamp" [13, 24]. This

conserved interaction pattern could also be reproduced for the CAR-SRC-1 model, where these residues match Lys177 (H3) and Glu345 (AF-2) (Fig. 5c). Lys177 forms a hydrogen bond with the backbone carbonyl group of Leu693 of SRC-1, whereas Glu345 interacts with the backbone amide groups of Ile689 and Leu690. Additional hydrogen bonds are also formed between His687 of SRC-1 and Lys195 (H4) and between His687 and Glu345. Furthermore, a hydrogen bond between a histidine residue on the coactivator and the conserved lysine (Lys177) is present in other nuclear receptors [21, 26, 27]. This interaction is also observed in the homology model and persisted during the entire MD simulation.

In order to analyze the activation mechanism of CAR upon agonist binding, the CAR-SRC-1 model was used for docking studies using the GOLD program [28]. The docking runs yielded 19 favored poses for clotrimazole grouped into two clusters that differed only slightly from each other. For TMPP, 18 poses were found, which are grouped in two clusters. The docking pose with the highest fitness score was selected for each ligand and investigated further by MD simulations.

Clotrimazole is bound deeply in the ligand-binding pocket (Fig. 6a). No direct contact between clotrimazole and the AF-2 domain is observed. The aromatic side chains of the ligand mainly interact with several aromatic residues of the binding pocket (Phe112, Phe161, Phe234 and Tyr326). During the 2.5 ns MD simulation, the position of clotrimazole did not change significantly. The distance between Tyr326 and Leu343 (AF-2) decreased (Table 1). Phe161 moved towards the interface between LBD and AF-2, establishing van-der-Waals interactions with Met339. The ligand-binding pocket was widened by a minor movement of the β4-strand in combination with small side-chain reorientations: residues His160 and Tyr224 maintained their hydrogen bond but were pushed towards the outside of the LBD, whereas Phe243 now points away from the ligand-binding pocket. These events increase the size of the pocket, resulting in a volume of 750 Å^3. TMPP shows a different binding mode (Fig. 6b). It is located much closer to the interface between LBD and AF-2 than clotrimazole. One of the methylphenyl groups interacts directly with Leu343 and Ile346 from AF-2. The two remaining methylphenyl groups point into the ligand-binding pocket, both interacting with Phe161 and pushing it deeper into the pocket. As a result, the distance to Met339 is increased as compared to the ligand-free receptor. Additional van-der-Waals interactions of the methylphenyl groups with Phe234 and Tyr326 could be observed. The phosphate group forms strong hydrogen bonds to both Asn165 and Tyr326 that remained stable during the entire MD simulation. Because of steric effects, TMPP provoked a reorientation of Val169 that resulted in an interaction with Ile346 from AF-2 (Fig. 6b). In agreement with the simulation of clotrimazole, the distance between Tyr326 and Leu343 (AF-2) also decreased in the simulation of TMPP (Table 1). The size of the ligand-binding pocket increased to a final volume of 560 Å^3.

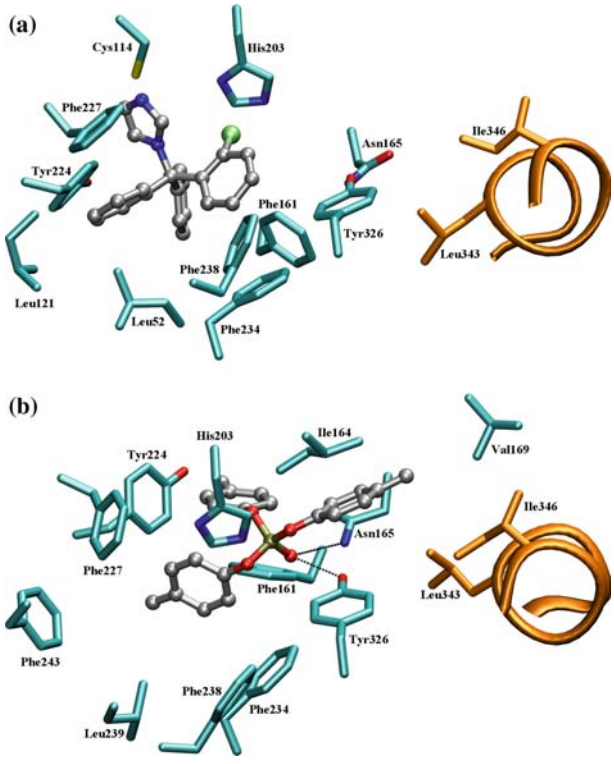

Fig. 6 Binding modes of CAR activators. **a** Clotrimazole (carbon atoms in *grey*) is positioned deeply in the LBD without any contact to the AF-2 helix (*orange*). Main interactions are observed with aromatic amino acids (Phe112, Phe161, Phe234 and Tyr326). Phe161 has moved towards the interface LBD/AF-2 enabling interaction with Met339 from the loop connecting H10/11 and AF-2. **b** TMPP (carbon atoms in *grey*) is located close to the AF-2-LBD interface establishing van-der-Waals interactions with Leu343 and Ile346 from AF-2. Additionally, hydrogen bonds with residues Asn165 and Tyr326 are observed. Phe161 is surrounded by two methylphenyl groups resulting in reorientation into the ligand binding pocket

Mutagenesis studies have shown that the single-point mutation Phe238Ala results in a loss of CAR basal activity (Fig. 7a), indicating a prominent role in the mechanism of constitutive activity. The Phe243Ala mutation also reduces the basal activity significantly. In order to prove the consistency between the experimental and theoretical studies, both mutants were modeled and analyzed by MD simulations. During simulation, the Phe238Ala mutation provoked rotation of the side chain of Tyr326 (around χ1) resulting in a more buried conformation of Tyr326 within the CBD (Fig. 7b). As a result, the interactions of Tyr326 with Leu343 and Ile346 were disrupted (Table 1). The hydrogen bond between Asn165 and Tyr326 was also lost. Phe161 shows weak interactions with Leu343 and is in close contact to Met339.

The mutation Phe243Ala forced H7 towards the β-sheet by more than 3 Å, and H10/11 was pushed in the same direction. These movements result in a pronounced reorientation of several residues in the ligand binding pocket (Fig. 7c). Tyr326 now points more deeply in the ligand-binding cavity and contact with AF-2 is lost

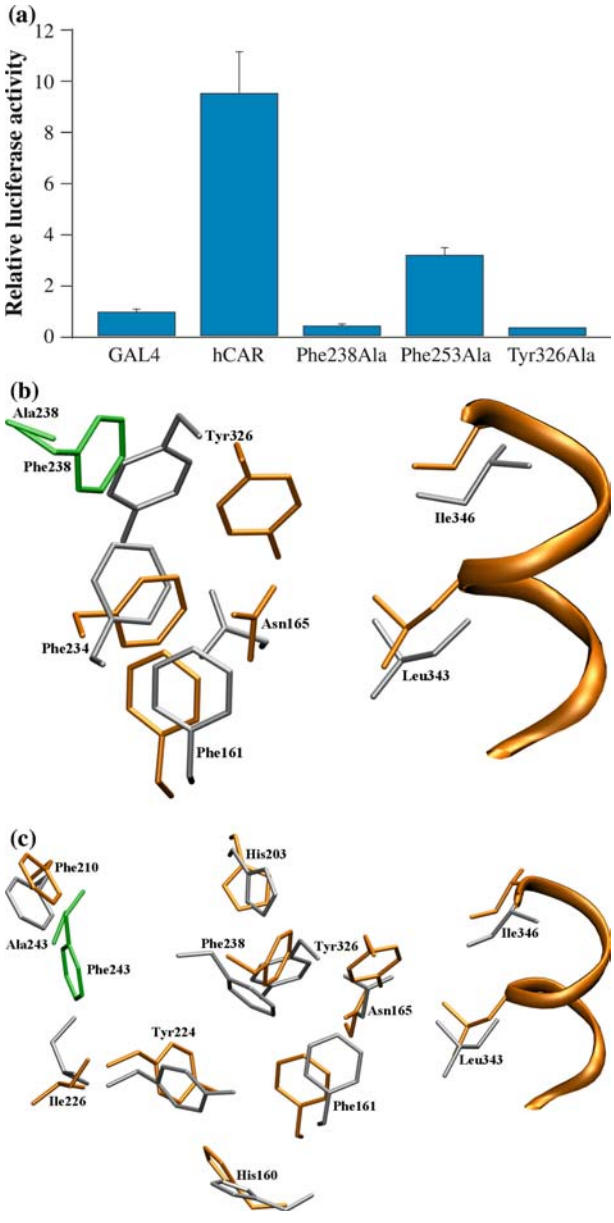

Fig. 7 Site-directed Mutagenesis. **a** Relative luciferase activity measured for CAR wildtype and three independent point mutations. Wildtype CAR is constitutively active whereas mutation of Phe238, Phe243 and Tyr326 results in decrease or loss of basal activity. **b** Mutation of Phe238 to alanine (both in *green*): during the MD simulations Tyr326 changed its position pointing now into the ligand binding pocket. Contacts between Tyr326 and AF-2 are disrupted and the hydrogen bond with Asn165 is lost. **c** Mutation of Phe243 to alanine (both in *green*) results in sidechain reorientation of several residues. Due to displacement of H10/11 Tyr326 now points into the ligand binding pocket. The hydrogen bond between Tyr224 and His160 is abolished resulting in rotation of Tyr224 into the ligand binding pocket

(Table 1). The conformation of Phe238 changed, resulting in loss of any stabilizing effects on Tyr326. The hydrogen bonds between Tyr326 and Asn165 as well as between His160 and Tyr224 were destroyed, provoking a rotation of the side chain of Tyr224 into the ligand-binding pocket.

Discussion

The AF-2 domain located at the C-terminal end is thought to be responsible for the activation of nuclear receptors. Supposedly, agonists and antagonists induce conformational changes of AF-2 that subsequently result in formation of a complex with coactivators or corepressors, respectively. In the case of the agonist-occupied binding site, AF-2 covers the ligand-binding pocket like a lid. In contrast to other nuclear receptors, CAR has substantial constitutive activity, but its structural basis is not yet clear. Using MD simulations of a homology model of CAR, we found evidence for a potential activation mechanism based on specific van-der-Waals interactions between the LBD and the AF-2 domain, which contribute to AF-2 remaining anchored to the LBD. Of several unique residues involved in these interactions, Tyr326 has been found to be of special importance. A cluster of hydrophobic and aromatic residues around Tyr326 fix the side chain to enable its van-der-Waals interactions with AF-2 residues. This has also been demonstrated by the calculated molecular interaction fields with GRID (Fig. 4b). Phe238, which is located in close proximity, seems to prevent rotation of the Tyr326 side chain around its $\chi 1$ angle and thus blocking Tyr326 from the ligand-binding pocket. Val199, His203, Phe234 and Ile330 are positioned above and below the plane of the Tyr326 side chain, thereby preventing rotation around $\chi 2$. In addition the orientation of Tyr326 is stabilized via a hydrogen bond with Asn165. Assisted by its surrounding residues, Tyr326 emerges as a central interaction partner for AF-2 and keeping it closely attached to the LBD. This interaction pattern seems to be unique among related nuclear receptors and thus provides a convincing explanation for constitutive activity of CAR. The critical role of Tyr326 in constitutive activity, was borne out experimentally: the Tyr326Ala mutant had lost its basal activity (Fig. 7a). Van-der-Waals interactions between LBD and AF-2 seem to be a common feature for constitutive activity, as seen in crystal structures of murine LRH-1 (Liver Receptor Homologue 1) and human ERR3 (Estrogen Related Receptor 3) [29, 30].

Further results are supported by data from site-directed mutagenesis: replacement of Phe238 for alanine reduced the basal activity significantly, and during the MD simulation, the position of Tyr326 changed and its van-der-Waals contacts with AF-2 were disrupted. The weaker interactions between LBD and AF-2 might lead to a reorientation of AF-2, disruption of the SRC-1 binding site, and finally to the reduction of basal activity. The CAR activity can also be modulated by residues more distant from the LBD/AF-2 interface: the mutation Phe243Ala resulted in a modification of the overall shape of the ligand-binding pocket that caused a displacement of H10/11 and a subsequent reorientation of Tyr326. Thus, we could explain the experimentally observed loss of basal activity on a structural level with models of mutated

receptors. This suggests that the current models and methods are applicable to generation of further hypotheses and experimental testing to elucidate CAR ligand specificity and mechanism of activation.

It has recently been reported that replacement of either Leu343 or Ile330 by Ala reduces the basal activity significantly [23]. This is in accord with our observations, where Leu343 is the only amino acid from AF-2 that permanently shows van-der-Waals interactions with LBD. Upon mutation to alanine, the contact to Tyr326 would be disrupted and the remaining interactions between Ile346 and the LBD might not be sufficient to keep AF-2 anchored to the active conformation. Mutation of Ile330 to alanine would not only reduce the hydrophobic surface area and the number of potential interaction partners for Leu343 but also destabilize the position of Tyr326, because Ile330 is one of the amino acids that restrain the side chain of Tyr326. This stabilization might be reduced by its mutation to alanine resulting in an increased flexibility for Tyr326 which might have implications on the stability of interactions with AF-2.

In the agonist-bound structures of PXR and VDR, van-der-Waals interactions between the ligand and the AF-2 domain have been observed (Fig. 8a, b) [20, 21]. These are believed to maintain AF-2 attached to the LBD, enabling coactivator binding when a ligand is present. We have shown that the single residue Tyr326 in CAR makes van-der-Waals contacts to AF-2. Tyr326 thereby accommodates a corresponding position relative to AF-2 as the ligands do in the PXR and VDR structures (Fig. 8c). We therefore infer that the constitutive activity of CAR may result from a ''molecular mimicry'' of a bound agonist.

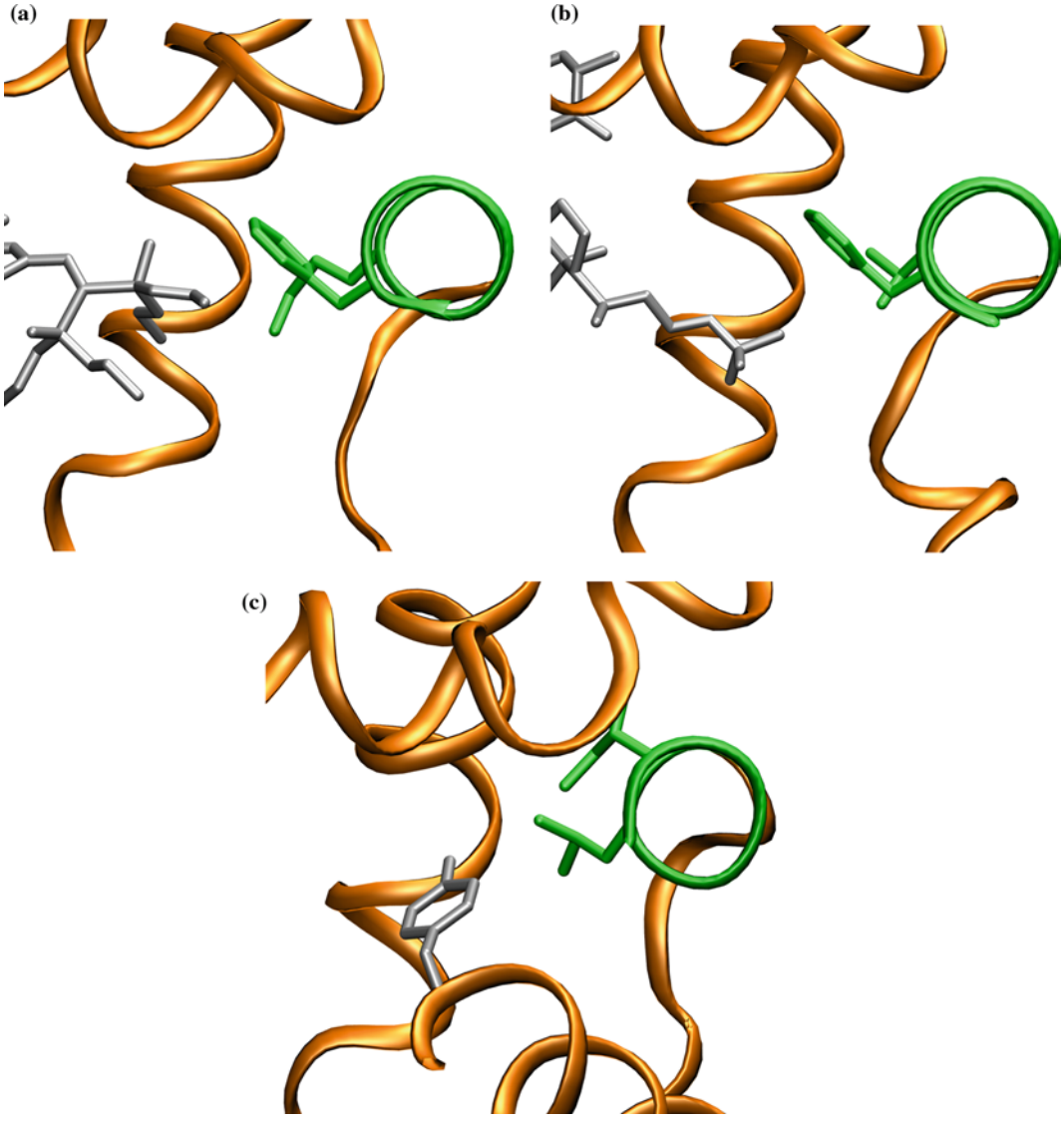

Fig. 8 ''Molecular mimicry''. Interaction between the AF-2 (*green*) and the LBD domain (*orange*) for PXR **(a)**, VDR **(b)** and CAR **(c)**. Ligands for PXR and VDR as well as the corresponding amino acid in CAR, Tyr326, are colored in *grey*. PXR and VDR exhibit van-der-Waals interactions between the bound ligand and residues located on AF-2 (*green*). In CAR a bound ligand is mimicked by Tyr326 that might lead to constitutive activity of CAR

Coactivator binding is essential for the ability to activate transcription. As a prerequisite, the AF-2 domain has to adopt a position that, together with residues of the remaining LBD, allows formation of a hydrophobic groove to which the coactivator can bind. We could show that the AF-2 domain in CAR is able to form this hydrophobic groove even in absence of any bound agonist.

Because of the limited flexibility of the AF-2 domain, the hydrophobic groove does not show a strictly defined geometry in the absence of the SRC-1 peptide. Thus, binding of SRC-1 seems to induce limited alterations on parts of the hydrophobic groove; especially the AF-2 domain is slightly reoriented. As a result, specific interactions between the LxxLL motif of SRC-1 and LBD/AF-2 occur, which are conserved among nuclear receptors [24, 25]. Existing van-der-Waals interactions between LBD and AF-2 are reinforced and additional contacts are introduced, which might contribute to keeping AF-2 in the new position.

Additionally, we observed a novel hydrogen bond between LBD (Gln331) and the ultimate C-terminal residue Ser348 in the presence of SRC-1. The influence on basal activity of human CAR remains to be elucidated. Localization of AF-2 in closer proximity to the LBD results in a small rotation of Tyr326 towards AF-2, which might be responsible for rotation of Phe161 towards the interface between LBD and AF2. Based on our observations, we propose a cooperative binding mode for SRC-1. The hydrophobic groove and additional residues involved in SRC-1 binding (e.g. Lys177, Lys195) exhibit considerable flexibility, resulting in a weak initial binding of SRC-1. After reorientation of several residues within the SRC-1 binding site (i.e. Phe161, Tyr326), specific interactions with AF-2 and LBD are established. The AF-2 domain is stabilized in this new position through novel interactions with the LBD that further enhance SRC-1 binding. Thermal denaturation experiments performed with PXR have shown that the overall stability of the LBD increases upon coactivator binding [21]. Our results suggest that this might be due to an enhanced interaction between LBD and AF-2.

Binding modes for structurally diverse ligands in the CAR binding site were obtained from docking procedures. For both clotrimazole and TMPP, one favorable binding mode was proposed. A similar conformation of clotrimazole in a CAR model was described in a previous study [31]. Both agonists used in this study have been shown to interact with amino acids surrounding Tyr326, leading to further stabilization of the tyrosine side chain. As a result, the distance between Tyr326 and Leu343 is decreased compared to the empty receptor (Table 1). This gives reason to propose an increase of the van-der-Waals interactions between LBD and AF-2, which might keep AF-2 in its new position, facilitating SRC-1 binding and further leading to increased CAR activity. Although the adopted binding modes of clotrimazole and TMPP are quite different, both ligands induce comparable structural changes that result in a further increase of CAR activity. Based on the observations for clotrimazole and TMPP binding, a general mechanism of the action of agonists could be proposed that is based on a further stabilization of favorable side-chain conformations, as previously described for the activation mechanism.

The function of CAR as a xenosensor requires recognition of a diverse set of ligands. Thus, the ability of the binding site to adapt to a variety of ligands is essential. Upon agonist binding, the ligand-binding pocket is able to expand up to 80%. Increasing the size of the cavity has also been reported for PXR complexed with hyperforin [32]. During our simulations, we observed two regions of moderate flexibility upon ligand binding. In contrast to PXR, structural adaptations took place within parts of the β-sheet (β4-strand) and a residue located at the interface LBD/AF-2 (Val169). The smaller ligand spectrum of CAR compared to PXR might thus be due to the significantly smaller ligand-binding pocket and the limited flexibility of regions located therein.

Several homology models of the human and mouse CAR LBD have been generated. These have given first insight into ligand binding and interactions between LBD and AF-2 [31, 33–35]. These models differ in several respects from the presented one. The ligand-binding pocket is much larger (1150–1170 vs. 480 $\mathring{A}^3$) than observed in our model. This might be due to the selection of PXR as the only template for the model generation and different orientations of side chains within the binding pocket [31, 33]. In contrast to previous studies, we performed MD simulations in order to account for the dynamic behavior of this complex system. The simulations gave insight into the formation of several new interactions that have been found to be critical for CAR activity and that have been supported by the mutagenesis studies described.

Conclusions

Our simulations have given new insight into the molecular basis of the constitutive activity of CAR. We proposed an activation mechanism based on specific van-der-Waals interactions between residues from the LBD and AF-2 domain. Functional consequences of LBD mutations could be reproduced or at least explained on a structural level. Nevertheless, information on the mechanism of action of antagonists is still lacking. Modeling of CAR in complex with corepressors might reveal the structural basis of CAR inactivation and will create a basis for the development of specific CAR inhibitors.

Materials and methods

Model building

Homology models of the human CAR ligand-binding domain with and without a bound coactivator (peptide

segment from SRC-1) were built using the homology module of INSIGHT II [36]. The sequence alignment was generated using CLUSTAL W [37]. The related crystal structures of PXR (pdb code 1NRL, resolution 2.0 Å, chains B and D) [21] and VDR (pdb code 1DB1, resolution 1.8 Å) [20] were taken as template structures for homology modeling. The corresponding segments from each template were chosen, as shown in Fig. 1a. Non-conserved sidechains were reoriented by SCWRL 2.95 [38].

MD simulations

A solvent box with dimensions 5.59×6.50×6.25 nm (CAR-SRC-1: 6.16×6.78×5.60 nm) was generated to simulate the models. The protonation state of the models was adjusted in order to mimic a pH value of 7.4. All water molecules were represented with the simple point charge (SPC) model [39]. 19 Na^+ and 15 Cl^- (CAR-SRC-1: 19 Na^+ and 16 Cl^-) counterions were added by replacing water molecules to ensure the overall neutrality of the simulated system. The total numbers of atoms in the two systems were 20795 (CAR) and 21505 (CAR-SRC-1). The models were minimized using 2000 steps of steepest descent with the GROMOS96 force field [40]. Molecular dynamics simulations with periodic boundary conditions were performed at 310 K using the program package GROMACS. The Particle-mesh-Ewald (PME) method was used for accurate determination of longe-range electrostatic interactions. VDW interactions were considered applying a cutoff of 0.9 nm. The time step for the simulations was 1 fs. To keep the system at constant temperature, a Berendsen thermostat was applied using a coupling time of 0.1 ps [41]. Constant pressure was maintained by coupling to an external bath with a reference value of 10^5 Pa, with a coupling time 1.0 ps and an isothermal compressibility of 4.5×10^{-10} Pa^{-1}.

For the model of CAR-SRC-1 an equilibration period of 250 ps with constraints of 1000 kJ mol^1 on the backbone atoms except for the H1–H3 loop was followed by a free MD simulation lasting 2.25 ns. Bonds between heavy atoms and corresponding hydrogen atoms were constrained to their equilibrium bond lengths using the LINCS algorithm. MD simulations of mutated forms of CAR-SRC-1 were carried out in the same way. CAR without coactivator was equilibrated with decreasing constraints (1000–100 kJ mol^{-1}) on the backbone for 400 ps followed by a free MD simulation lasting 2 ns. The trajectories of the free MD simulations were analyzed using NMRCLUST [42]. Resulting clusters were examined and representative frames were selected and minimized with GROMACS. The stereochemical quality of the models was evaluated using PROCHECK [43] and PROFILES-3D [44]. The size of the ligand binding cavity was determined by rolling a probe of 1.4 Å over the van-der-Waals surface using the program SURFNET [45]. Ligands were built within SYBYL 6.9 considering the protonation state at pH 7.4 and minimized applying the TRIPOS force field and default settings [46].

Molecular interaction fields

The molecular interaction potentials of the AF-2-binding domain were analyzed using the program GRID (Version 21) [47]. GRID is an approach to predict non-covalent interactions between a molecule of known three-dimensional structure (i.e. the CAR structure) and a small group as a probe (representing chemical features of the binding partner). The calculations were performed using the AF-2-truncated CAR structure. The calculations were performed on a cube (20×20×20 Å, spacing 1 Å) including the AF-2-binding region in order to search for interaction regions between CAR and the AF-2 domain. The GRID contour map obtained using the methyl C3 probe (indicating van-der-Waals interactions) was then viewed superimposed on the CAR structure using the SYBYL 6.9 software.

GOLD docking

Docking procedures for CAR-SRC-1 were performed with GOLD [28]. Goldscore was chosen as fitness function. For each ligand, docking runs were performed with a maximum allowed number of 30 poses. The poses obtained for each ligand were grouped into several unique binding modes. The solution with the highest fitness score was chosen for further examination. Subsequent MD simulations were performed with the settings described previously. Missing parameters for the ligands were obtained manually using the GROMOS96 topology. Figures were prepared using VMD [48].

DNA plasmids and cotransfection assays

The CMV promoter-driven GAL4-human CAR LBD fusion plasmid has been described [17]. Mutations were done according to instructions in the QuickChange kit (Stratagene, La Jolla, CA, USA). UAS_4-tk-luc and pCMV plasmids as well as cotransfection assays have been described [18]. Luciferase activities were normalized to β-galactosidase activity and expressed as means ± standard deviation from three or four independent experiments.

References

1. Guengerich FP (1989) Annu Rev Pharmacol Toxicol 29:241–263
2. Turkey RH, Strassburg CP (2000) Annu Rev Pharmacol Toxicol 40:581–616
3. Borst P, Oude Elferink R (2002) Annu Rev Biochem 71:537–592
4. Okey AB (1990) Pharmacol Ther 45:241–298

5. Willson TM, Kliewer SA (2002) Nat Rev 1:259–266
6. Baes M, Gulick T, Choi HS, Martinoli MG, Simha G, Moore DD (1994) Mol Cell Biol 14:1544–1551
7. Kliewer SA, Moore JT, Wade L, Staudinger JL, Watson MA, Jones SA, McKee DD, Oliver BB, Willson TM, Zetterstrom RH, Perlmann T, Lehmann JM (1998) Cell 92:73–82
8. Laudet V, Gronemeyer H (2002) The nuclear receptor factsbook. Academic Press, London
9. Moras D, Gronemeyer H (1998) Curr Opin Cell Biol 10:384–391
10. McKenna NJ, Lanz RB, O'Malley BW (1999) Endocr Rev 20:321–344
11. Honkakoski P, Zelko I, Sueyoshi T, Negishi M (1998) Mol Cell Biol 1:5652–5658
12. Ueda A, Hamadeh HK, Webb HK, Yamamoto Y, Sueyoshi T, Afshari CA, Lehmann JM, Negishi M (2002) Mol Pharmacol 61:1–6
13. Nolte RT, Wisely GB, Westin S, Cobb JE, Lambert MH, Kurokawa R, Rosenfeld MG, Willson TM, Glass CK, Milburn MV (1998) Nature 395:137–143
14. Maglich JM, Parks DJ, Moore LB, Collins JL, Goodwin B, Billin AN, Stoltz CA, Kliewer SA, Lambert MH, Willson TM, Moore JT (2003) J Biol Chem 278:17277–17283
15. Honkakoski P, Palvimo JJ, Penttila L, Vepsäläinen J, Auriola S (2004) Biochem Pharmacol 67:97–106
16. Toell A, Kröncke KD, Kleinert H, Carlberg C (2002) J Cell Biochem 85:72–82
17. Mäkinen J, Frank C, Jyrkkärinne J, Gynther J, Carlberg C, Honkakoski P (2002) Mol Pharmacol 62:366–378
18. Jyrkkärinne J, Makinen J, Gynther J, Savolainen H, Poso A, Honkakoski P (2003) J Med Chem 46:4687–4695
19. Watkins RE, Wisely GB, Moore LB, Collins JL, Lambert MH, Williams SP, Willson TM, Kliewer SA, Redinbo MR (2001) Science 292:2329–2333
20. Rochel N, Wurtz JM, Mitschler A, Klaholz B, Moras D (2000) Mol Cell 5:173–179
21. Watkins RE, Davis-Searles PR, Lambert MH, Redinbo MR (2003) J Mol Biol 331:815–828
22. Andersin T, Väisänen S, Carlberg C (2003) Mol Endocrinol 17:234–246
23. Frank C, Molnar F, Matilainen M, Lempiainen H, Carlberg C (2004) J Biol Chem 279:33558–33566
24. Darimont BD, Wagner RL, Apriletti JW, Stallcup MR, Kushner PJ, Baxter JD, Fletterick RJ, Yamamoto KR (1998) Genes Dev 12:3343–3356
25. Feng W, Ribeiro RC, Wagner RL, Nguyen H, Apriletti JW, Fletterick RJ, Baxter JD, Kushner PJ, West BL (1998) Science 280:1747–1749
26. Xu HE, Lambert MH, Montana VG, Plunket KD, Moore LB, Collins JL, Oplinger JA, Kliewer SA, Gampe Jr RT, McKee DD, Moore JT, Willson TM (2001) Proc Natl Acad Sci USA 98:13919–13924
27. Gampe Jr RT, Montana VG, Lambert MH, Miller AB, Bledsoe RK, Milburn MV, Kliewer SA, Willson TM, Xu HE (2001) Mol Cell 5:545–555
28. GOLD Version 2.1 (2003) CCDC, Cambridge, UK
29. Sablin EP, Krylova IN, Fletterick RJ, Ingraham HA (2003) Mol Cell 11:1575–1585
30. Greschik H, Wurtz JM, Sanglier S, Bourguet W, van Dorsselaer A, Moras D, Renaud JP (2002) Mol Cell 9:303–313
31. Xiao L, Cui X, Madison V, White RE, Cheng KC (2003) Drug Metab Dispos 30:951–956
32. Watkins RE, Maglich JM, Moore LB, Wisely GB, Noble SM, Davis-Searles PR, Lambert MH, Kliewer SA, Redinbo MR (2003) Biochemistry 42:1430–1438
33. Dussault I, Lin M, Hollister K, Fan M, Termini J, Sherman MA, Forman BM (2002) Mol Cell Biol 22:5270–5280
34. Moore JT, Moore LB, Maglich JM, Kliewer SA (2003) Biochim Biophys Acta 1691:235–238
35. Jacobs MN, Dickins M, Lewis DFV (2003) J Steroid Biochem Mol Biol 84:117–132
36. INSIGHT II (2000) MSI, San Diego, USA
37. Higgins D, Thompson J, Gibson T, Thompson JD, Higgins DG, Gibson TJ (1994) Nucleic Acids Res 22:4673–4680
38. Bower MJ, Cohen FE, Dunbrack Jr LR (1997) J Mol Biol 267:1268–1280
39. Berendsen HJC, Postma JPM, van Gunsteren WF, Hermans J (1981) Interaction models for water in relation to protein hydration. In: Pullman B (ed) Intermolecular forces. Reidel, Dordrecht, pp 331–342
40. GROMACS Version 3.1.4 (2002) BIOSON Research institute and laboratory of biophysical chemistry, University of Groningen, The Netherlands
41. Berendsen HJC, Postma JPM, DiNola A, Haak JR (1984) J Chem Phys 81:3684–3690
42. Kelley LA, Gardner SP, Sutcliffe MJ (1996) Prot Eng 9:1063–1065
43. Laskowski RA, MacArthur MW, Moss DS, Thornton JM (1993) J Appl Cryst 26:283–291
44. Fischer D, Eisenberg D (1999) Curr Opin Struct Biol 9:208–211
45. Laskowski RA (1995) J Mol Graph 13:323–330
46. Sybyl 6.9 (2003) Tripos Inc., St. Louis, USA
47. GRID21 (2003) Moldiscovery Ltd. Pinner, Middlesex, UK
48. Humphrey W, Dalke A, Schulten K (1996) J Mol Graph 14:33–38